Enhancing Transient Stability of Distribution Networks With Massive Proliferation of Converter-Interfaced Distributed Generators

Mohsen Tajdinian, Mehdi Zareian Jahromi, Mohammad Hasan Hemmatpour, Payman Dehghanian, *Member, IEEE*, Miadreza Shafie-khah, *Senior Member, IEEE*, and João P. S. Catalão, *Senior Member, IEEE*

***Abstract*—High penetration of renewable energy sources and energy storage systems has considerably increased the flexibility in power distribution networks operation. However, employing converter-interfaced energy and storage sources may significantly reduce the mechanical inertia and as a result, the power grids may confront serious stability challenges during transient conditions. This article introduces a strategy for enhancing transient stability margin of active distribution networks with high penetration of electric vehicles (EVs). The proposed optimization strategy intends to control EVs contributions during transient stability conditions. The EVs contributions are controlled through a new index proposed based on the system's total corrected critical kinetic energy (TCCKE). The proposed procedure for TCCKE calculation is driven by a hybrid algorithm taking into account the equal area criterion and sensitivity analysis. The suggested procedure for TCCKE only depends on the during fault data and as a result, the proposed optimization strategy is useful to prevent transient instability in the case of first swing instability. The proposed optimization is applied and evaluated on the IEEE test systems. The results clearly demonstrate the applicability and efficacy during a multitude of fault and emergency conditions.**

***Index Terms*—Converter-interfaced, distributed generation, electric vehicle (EV), optimization, transient stability.**

Manuscript received August 10, 2020; revised October 20, 2020; accepted December 5, 2020. The work of Miadreza Shafie-khah was supported by the Business Finland through SolarX Research Project, 2019–2021, under Grant 6844/31/2018. The work of João P. S. Catalão was supported in part by FEDER funds through COMPETE 2020 and in part by the Portuguese funds through FCT under Grant POCI-010145-FEDER029803 (02/SAICT/2017). *(Corresponding authors: Miadreza Shafie-khah; João P. S. Catalão.)*

Mohsen Tajdinian is with the School of Electrical and Computer Engineering, Shiraz University, Shiraz 84334–71946, Iran (e-mail: tajdinian.m@shirazu.ac.ir).

Mehdi Zareian Jahromi is with the Department of Electrical Engineering, Amirkabir University of Technology, Tehran 1591634311, Iran (e-mail: m.jahromi@aut.ac.ir).

Mohammad Hasan Hemmatpour is with the Department of Electrical Engineering, Jahrom University, Jahrom 7413188941, Iran (e-mail: m.h.hemmatpour@jahromu.ac.ir).

Payman Dehghanian is with the Department of Electrical and Computer Engineering, The George Washington University, Washington DC 20052 USA (e-mail: payman@gwu.edu).

Miadreza Shafie-khah is with the School of Technology and Innovations, University of Vaasa, 65200 Vaasa, Finland (e-mail: mshafiek@uva.fi).

João P. S. Catalão is with the Faculty of Engineering, University of Porto, 4099-002 Porto, Portugal, and also with INESC TEC, 4200-465 Porto, Portugal (e-mail: catalao@fe.up.pt).

Digital Object Identifier 10.1109/JSYST.2020.3043378

NOMENCLATURE

The list of parameters, acronyms and abbreviations in this article is as follows.

CBC	Converter-based connected.
CDGs	Converter-interfaced distributed generators.
CKE	Critical kinetic energy.
DG	Distributed generation.
EAC	Equal area criterion.
ESSs	Energy storage systems.
LDG	Less disturbed generator.
OF	Objective function.
PCC	Point of common coupling.
PEV	Plug-in electric vehicle.
PV	Photovoltaic.
RES	Renewable energy source.
SDG	Severely disturbed denerator.
TCCKE	Total corrected critical kinetic energy.
VSG	Virtual synchronous generator.
δ_{VSG}	Phase angle of the internal voltage.
ω_{VSG}	Virtual angular speed.
ω_0	Rated angular speed.
P_m	Reference active power.
P_{VSG}	Active power output of VSG.
Q_m	Reference reactive power.
Q_{VSG}	Reactive power output of VSG.
E'_{VSG}	RMS value of the internal potential.
V_{PCC}	RMS voltage at PCC.
X'_f	Filter impedance.
τ_{VSG}	Time constant of VSG.
J_p	Damping coefficient of VSG.
$\tau_{K,i}$	Time constant related to reactive power loop.
J_q	Damping coefficient related to the voltage control loop.
δ_0	Prefault operating point.
δ_c	Critical clearing point.
$\delta_{\max}$	Post fault operating point.
$Ke(t)$	Time domain kinetic energy.

I. INTRODUCTION

WITH the growing concerns over environmental challenges of the conventional fossil-fueled power plants,

the penetration rate of renewable energy sources (RESs) has been extensively enhanced in electric power systems worldwide. Wind- and solar- energies serve the highest contribution to the total share of RESs [1], [2]. The majority of RESs are connected to power grids through power electronic interfaces. Additionally, power electronic interfaces have also been widely utilized due to their application in energy storage systems (ESSs) and electric vehicle (EV) stations which have been growingly applied in smart distribution grids. Due to no mechanical inertia, employing power electronic interfaces connected RESs have brought challenges the power system security. Compared to bulk interconnected power systems, such impacts more profoundly affect active distribution grids, since for representing less strength [3], [4]. This article discusses the contribution of converter-based connected (CBC) power generation and energy storage on the dynamic security of the power distribution systems.

Due to power system deregulations owing to proliferation of RESs, power system dynamic security assessment, and transient stability challenges have drawn lots of attention in recent years [5], [6]. Transient stability discusses the ability of preserving synchronism between generators when the system is subjected to a large perturbation. Such a large perturbation on transmission grids may result in a widespread blackout. Considering the rapidly increasing integration of large-scale rotational wind turbines in power transmission grids, the transient stability analysis of both synchronous and asynchronous generators has been addressed in many recently published works [7]–[9]. Concentrating on the distribution networks, it can be observed that due to remarkably enhancement of directly connected RESs to distribution network, the significance of active distribution networks impact on the instability of the system in the event of a large perturbation in the grid has become a challenging issue.

With the rushing arrival of power electronic-interfaced distributed energy resources (DERs), such as photovoltaic farms (PV), ESSs and EV stations, the contribution of CBC power generation to the traditional transient stability measures have become more critical [10], [11]. The role of the CBC power generations has been addressed in several publications [12]–[15], where the focus has been primarily on both transient stability and frequency stability analysis. Various algorithms have been presented to design optimal frequency control mechanisms by monitoring and managing the virtual inertia of DERs. However, the transient stability enhancement of active distribution networks with high penetration of CBC power generations and storage systems have not been fully investigated.

Among CBC storage systems, EVs stations are considered as the storages that provide power to charge EVs and plug-in hybrid EVs batteries for vehicular operation. Concentrating on active distribution networks, research studies have reported that as the number of EVs increases, the uncertainty in load, power losses, and voltage profile across the system will also dramatically change. As a result, the integration of large-scale EVs significantly impacts the power distribution grid operation. Several research studies have been conducted to address the EV charging mechanisms and the optimal allocation of charging stations considering distribution grid constraints [16]–[19]. Optimal algorithms for allocation and control of the ESSs are also presented with the main goal to achieve an optimal frequency control in islanded microgrids [20]–[22].

Some research studies are conducted for the impact of gridable vehicles (GVs) and ESSs on the improvement of the power quality and transient stability at local transmission power systems [23]–[27]. These investigations reveal that charging/discharging facilities such as parking lots, public areas, and communities can improve the transient stability margin of the power system. Specifically, in [27], it has been suggested the use of GVs in a combination of superconducting magnetic energy storage (SMES) to enhance the transient stability of transmission level power system. While both GVs and SMES have the distinctive merit of fast response and are also able to control the power system's active and reactive power simultaneously with low losses and low toxic emissions, it should be noted that SMES is rather costly and can only afford to store a limited amount of energy. However, the majority of the past works on EVs are mainly concerned with the static and economic aspects of the EV contributions to the distribution grid, with no or minimum discussions on their impacts on the transient stability.

In this article, we investigate the problem of preserving transient stability in active distribution networks with high proliferation of PEVs. This article specifically concentrates on the control of PEVs during transient stability conditions while maintaining the optimal performance during normal operating conditions. As a matter of fact, this article aims to study the deterioration of transient stability due to the high penetration of CBC RESs.

The following contributions are highlighted in this article.

1) In order to mathematically model the transient stability in power distribution grids with PEVs, the concept of virtual synchronous generator (VSG) is employed.
2) An index based on the total critical corrected kinetic energy (TCCKE) is proposed, simultaneously reflecting the impacts of effective kinetic energy of all VSGs. TCCKE assessment is conducted in three stages: an assessment of the critical kinetic energy (CKE) using the proposed equal area criterion (EAC) is conducted first for each individual VSG; the assessment of the corrected CKE (CCKE) to capture the effects of fault trajectory and topology changes is next pursued using the proposed sensitivity analysis; finally, the TCCKE is quantified to find the transient stability response of the entire distribution network.
3) Founded on the proposed TCCKE measure, a new OF is presented in which the contribution of the EV charging station during fault conditions is controlled so as to improve the transient stability margins.

The rest of the article is organized as follows. Section II discusses transient stability modeling requirement of EVs and introduces the mathematical formulations for TCCKE. The descriptions regarding the suggested OF and constraints are discussed in Section III. Evaluation and verification of the proposed approach are presented in Section IV. Concluding remarks are eventually provided in Section V.

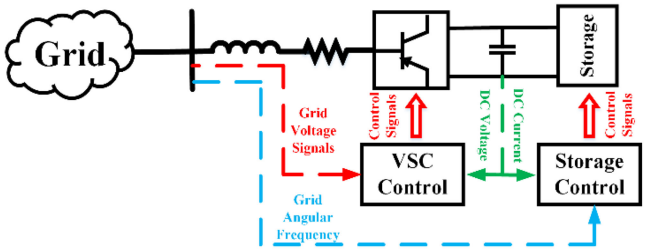

Fig. 1. General structure of EV storage station connected to distribution grid.

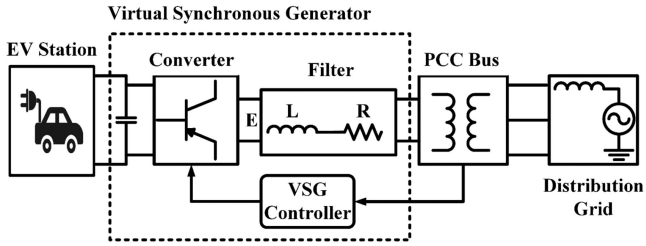

Fig. 2. General structure of a VSG.

II. Transient Stability Problem in Converter Interfaced Power Source

The active power distribution systems are featured more and more with asynchronous and converter-interfaced generating units, rather than synchronous generators. Also, significant penetration ESSs and EVs in active distribution networks may result in poor transient stability performance due to the less mechanical inertia of CBC generating units [28]–[29].

This article aims to enhance the robustness of the active distribution networks during transient stability conditions. We specifically aim at controlling the EV charging stations during faults so that a maximum transient stability strength can be achieved. To such aim, the following sections have provided the modeling of ESS for transient stability VSG concept which are employed in the proposed solution.

A. EV Charging Station Structure

With a myriad of commercial technologies available in the market, modeling ESSs has remained a complicated and challenging task. So far, several studies have addressed the ESS modeling in economic and electricity market applications [16], [17]. This section is focused on the battery energy storage system (BESS) models that can be used in the transient stability analysis. In this regard, authors in [30] presented a generic VSC-based model for ESSs, illustrated in Fig. 1.

The general goal for an ESS here is to control the system frequency compared with the center of inertia frequency or to manage the power flows in the transmission lines.

To accomplish modeling the ESS presented in Fig. 1, it is required to derive a dynamic model for BES. Shepherd model of BES is known as the most commonly used for representing a rechargeable battery in dynamic analysis.

The Shepherd model for BES is mathematically expressed as follows [30]:

$$\frac{dq_e}{dt} = \frac{i_b}{3600} \tag{1a}$$

$$\frac{di_m}{dt} = \frac{i_b - i_m}{\tau_m} \tag{1b}$$

$$0 = v_{oc} - v_p(q_e, i_m) + v_e e^{-\zeta q_e} - r_i i_b - v_b \tag{1c}$$

$$v_p(q_e, i_m) = \begin{cases} \frac{r_p i_m}{q_e + \varepsilon} + \frac{k_p q_e}{SoC} & charge\ mode \quad (i_m \le 0) \\ \frac{r_p i_m + k_p q_e}{SoC} & discharge\ mode \quad (i_m > 0) \end{cases} \tag{1d}$$

$$SoC = \frac{q_n - q_e}{q_n}. \tag{1e}$$

Note that expression (1) is that the nonlinearity of v_p generally results in two different sets of equations. Hence, depending on the state of the BES, the mathematical model is able to cover both BES operation modes. The modeling given in [30] is suitable for time domain transient stability analysis of the BESS. However, for the goals of this article, it is mandatory to use power-angle characteristics of BESS which is described in the following section.

B. Concept of VSG

The concept of VSG is introduced as a flexible strategy for controlling power electronic converters in grid-connected and stand-alone applications. Several VSG implementations have been proposed, with the emulation of inertia and damping of a traditional synchronous generator as their common feature. The implementations are mostly performed considering system nonlinearity in synchronous reference frame [31]–[32]. However, as discussed, the aim of this algorithm is to find a strategy to control the contribution of EVs so that the transient stability of the system is preserved. To take into account the DGs and EVs for calculating TCCKE, the representation of VSG concept in [33] is used to obtain *P*-δ equation form.

A general structure of a VSG connected to a three-phase power distribution network is shown in Fig. 2. The structure consists of a set of inverters/converters that transmit the power between dc and ac sides through a filter. Also, the transformer shown in Fig. 2 can be used as a coupling between the EV charging station as BESS and the distribution grid [33]. As one can see in Fig. 2, a control unit named VSG control covers two control loops including the active power control loop (*P*-δ) and reactive power control loop (*Q*-*V* droop).

In [31], the dynamic mathematical equations of VSG are expressed as follows taking into account the VSG controller:

$$\dot{\delta}_{vsg} = \omega_0(\omega_{vsg} - 1) \tag{2a}$$

$$\tau_{vsg}\dot{\omega}_{vsg} = P_m - P_{vsg} - J_p(\omega_{vsg} - 1) \tag{2b}$$

$$\tau_k \dot{E'}_{vsg} = Q_m - Q_{vsg} - J_q(V_{pcc} - 1) \tag{2c}$$

$$P_{vsg} = \frac{E'_{vsg} V_{pcc}}{X'_{filter}} \sin(\delta_{vsg} - \theta_{pcc}) \tag{2d}$$

$$Q_{vsg} = \frac{E'^2_{vsg} - E'_{vsg} V_{pcc} \cos(\delta_{vsg} - \theta_{pcc})}{X'_{filter}}. \tag{2e}$$

It should be noted that δ_{vsg}, ω_{vsg} , P_m, P_{vsg} , Q_m, Q_{vsg}, E'_{vsg}, and V_{pcc} are in per-unit values.

III. Proposed Strategy

To evaluate the TCCKE in the active distribution networks, it is essential to first assess the critical corrected kinetic energy of each EV charging station.

The critical corrected kinetic energy of each EV charging station is assessed in two stages: 1) an initial guess of the CKE based on the EAC and the single machine infinite bus concept; and 2) assessment of the critical corrected kinetic energy based on the proposed sensitivity analysis to consider the effects of fault trajectories.

A. Assessment of CKE

In order to calculate the critical corrected kinetic energy, the CKE of each individual VSG is first evaluated. Critical corrected kinetic energy is defined as the kinetic energy for three-phase fault to ground at the PCC bus. Therefore, it can be assumed that the electrical output power of the VSG (P_{vsg}) is almost equal to zero. Also the mechanical input power ($P_{m,i}$) is assumed almost constant in transient stability studies [7]. Applying the EAC on the three-phase fault at the PCC terminal, the following can be concluded:

$$\int_{\delta_0}^{\delta_c} P_m d\delta_{vsg} = \int_{\delta_c}^{\delta_{\max}} (P_{vsg} - P_m) d\delta_{vsg}. \tag{3}$$

According to (2), during fault, the electrical output power of VSG (P_{vsg}) to the power grid is represented as follows:

$$P_{vsg} = \frac{E'_{vsg} V_{pcc}}{X'_{filter}} \sin(\delta_{vsg} - \theta_{pcc}). \tag{4}$$

Substituting (4) in (3) and simplifying the integration (3), the following can be achieved:

$$P_m(\delta_c - \delta_0) = \frac{E'_{vsg} V_{pcc}}{X'_{filter}} \left(\cos(\delta_{\max} - \theta_{pcc}) - \cos(\delta_c - \theta_{pcc})\right) - P_m(\delta_{\max} - \delta_c). \tag{5}$$

In [8], it has been demonstrated that $\delta_{\max}$ can be assumed as $\pi - \delta_0$. As a result, the clearing angle is calculated from expression (5) as follows:

$$\delta_c = \cos^{-1}\left(\begin{array}{c}\cos(\pi - \delta_0 - \theta_{pcc}) \\ + \frac{X'_{filter} P_m}{E'_{vsg} V_{pcc}} (2\delta_0 - \pi)\end{array}\right) + \theta_{pcc}. \tag{6}$$

From (6), the CKE is assessed as follows [8], [9]:

$$Ke_{crit} = P_m(\delta_c - \delta_0). \tag{7}$$

B. Correction of CKE Accounting for Fault Trajectories

As mentioned earlier, the CKE metric is calculated for fault scenarios near generating units. However, fault location is variable, which may in turn result in significant variations in CKE. Hence, taking into account the effect of fault trajectory is critical. In so doing, this article proposes to evaluate the critical corrected kinetic energy as follows:

$$Ke^{corr}_{crit} = Ke_{crit} + \frac{\partial Ke_{crit}}{\partial Z} \tag{8}$$

where Z is an interim variable, reflecting the impact of the fault location. From (8), it can be found that E'_{vsg} and V_{pcc} vary for each fault trajectory. As a result, the CKE sensitivity to the fault trajectory is computed as follows:

$$\frac{\partial Ke_{crit}}{\partial Z} = \frac{\partial Ke_{crit}}{\partial E'_{vsg}} + \frac{\partial Ke_{crit}}{\partial V_{pcc}} = \frac{X'_{filter} P_m \left(\frac{1}{V_{pcc}} + \frac{1}{E'_{vsg}}\right)}{(V_{pcc} \times E'_{vsg}) \sqrt{1 - \left(\cos(\pi - \delta_0) + \frac{X'_{filter} P_m}{E'_{vsg} V_{pcc}} (2\delta_0 - \pi)\right)^2}}. \tag{9}$$

According to (9), critical corrected kinetic energy is calculated as follows:

$$Ke^{corr}_{crit} = Ke_{crit} + \frac{\partial Ke_{crit}}{\partial Z} = Ke_{crit} + \frac{X'_{filter} P_m \left(\frac{1}{V_{pcc}} + \frac{1}{E'_{vsg}}\right)}{(V_{pcc} \times E'_{vsg}) \sqrt{1 - \left(\cos(\pi - \delta_0) + \frac{X'_{filter} P_m}{E'_{vsg} V_{pcc}} (2\delta_0 - \pi)\right)^2}}. \tag{10}$$

C. Total Critical Corrected Kinetic Energy

During a disturbance, not all generators contribute to the instability of the system [6]. In other words, there are two sets of generators that contribute to the instability of the system during a disturbance. The first group of generators that contribute to system instability are named as severely disturbed generators (SDGs), while the other group of generators with less sensitivity are named less disturbed generators (LDGs).

The members of SDGs and LDGs are different in any realization of fault scenarios (location). In [6], a criterion based on the rotor speed and acceleration are introduced to identify the system SDGs and LDGs. With the SDGs and LDGs known, the TCCKE metric can be obtained as follows:

$$TKe^{corr}_{crit} = \frac{1}{2} J_{vsg,eq} \times (\omega^{crit}_{vsg,eq})^2 \tag{11}$$

$$J_{vsg,SDG} = \sum_{i=1}^{n_{SDG}} J_{vsg,i} \tag{12a}$$

$$J_{vsg,LDG} = \sum_{i=1}^{n_{LDG}} J_{vsg,i} \tag{12b}$$

$$J_{vsg,eq} = \frac{J_{vsg,SDG} \times J_{vsg,LDG}}{J_{vsg,SDG} + J_{vsg,LDG}} \tag{12c}$$

$$\omega^{crit}_{vsg,SDG} = \frac{\sum_{i=1}^{n_{SDG}} J_{vsg,i} \omega^{crit}_{vsg,i}}{\sum_{i=1}^{n} J_{vsg,i}} \tag{13a}$$

$$\omega^{crit}_{vsg,LDG} = \frac{\sum_{i=1}^{n_{LDG}} J_{vsg,i} \omega^{crit}_{vsg,i}}{\sum_{i=1}^{n_{LDG}} J_{vsg,i}} \tag{13b}$$

$$\omega^{crit}_{vsg,eq} = \omega^{crit}_{vsg,SDG} - \omega^{crit}_{vsg,LDG}. \tag{13c}$$

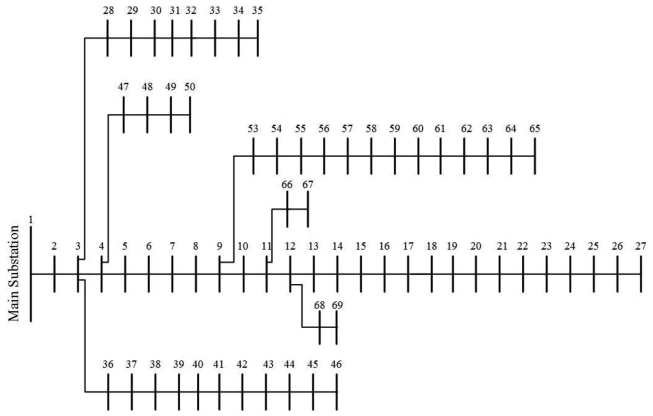

Fig. 3. IEEE 69-bus test system.

D. Implementation

One can see in the procedure of TKe_{crit}^{corr} assessment, the TCCKE can be updated in each time-step of simulation. Increasing the TKe_{crit}^{corr} results in an enhanced ability of the active distribution system to withstand the short circuit faults. One approach to control TKe_{crit}^{corr} is controlling the kinetic energy of the generators. This article proposes a new objective function which can help control the contribution of the system generations by modifications in the state of charge (SoC).

The proposed objective function is as follows:

$$OF = Minmization\ \{\alpha_1 f_1 + \alpha_2 f_2\} \tag{14}$$

$$f_1 = \frac{TKe_{crit}}{TKe_{crit}^{corr}} \tag{15}$$

$$f_2 = \sum_{i=1}^{N_G} \frac{\Delta Ke_i(t)}{Ke_{crit,i}} \tag{16}$$

$$\alpha_1 + \alpha_2 = 1. \tag{17}$$

With the proposed OF being minimized, the system strength in withstanding the fault scenarios will be maximized and as a result, the ability of each EV parking station to preserve the transient stability will be enhanced.

IV. Simulation Results and Discussions

This section provides discussions on the performance of the proposed objective function in dealing with transient stability conditions in active distribution networks with high integration of EV charging stations. The performance of the proposed scheme is comprehensively validated utilizing two IEEE distribution networks including IEEE 33-bus, IEEE 69-bus, and IEEE 119-bus test systems. The specifications of the test systems are adopted from [5], [8], [34], [35], and [36].

In the IEEE 33-bus test system, there are three DGs (including wind turbine and PV panels) and one EV charging stations. For the IEEE 69-bus test system, there are six DGs and three EV charging stations. Finally, ten DGs and five EV charging stations are considered in the IEEE 119-bus test system. The schematics of the test systems and data of DGs are provided in the Figs. 3 –5 and Tables I–V.

In order to ensure preserving the voltage constraints as desired, the optimal allocation algorithm in [37] is applied in each test system to find the optimal size and location of DGs and

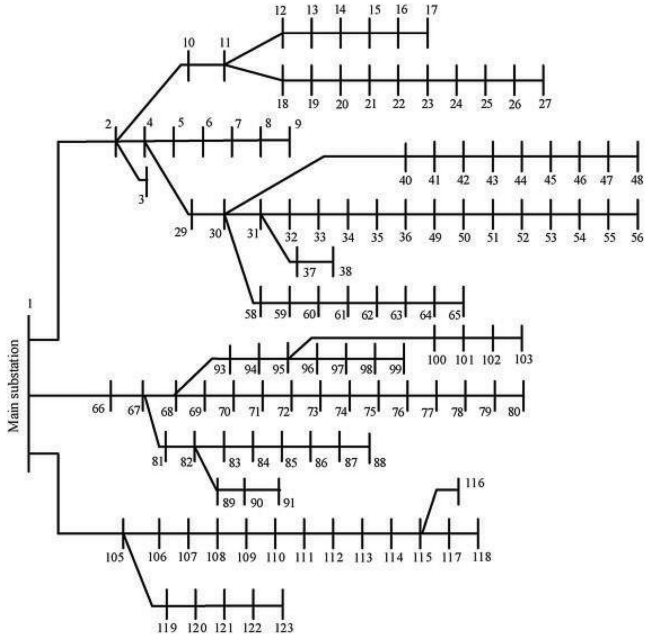

Fig. 4. IEEE 119-bus test system.

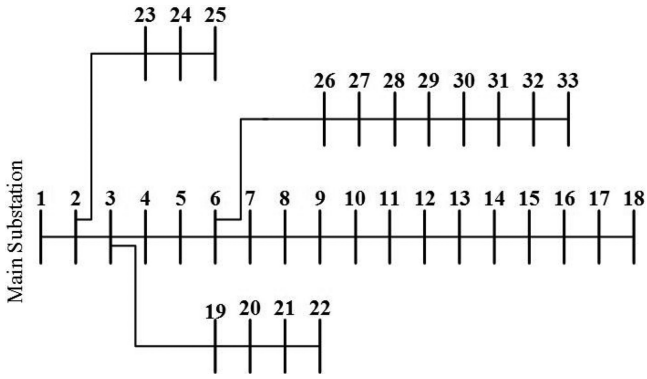

Fig. 5. IEEE 33-bus test system.

TABLE I
Generator Data

Nominal power (MW)	1.5
Frequency	60
Stator Resistance (R_s (pu))	0.00706
Stator Inductance (L_{ls} (pu))	0.171
Rotor Resistance ($R_{r'}$ (pu))	0.005
Rotor Inductance ($L_{lr'}$ (pu))	0.156
Magnetization Inductance (Lm (pu))	2.9
Inertia Constant (S)	5.04
Friction Factor	0.01
Pairs of Poles	4

TABLE II
TURBINE DATA

Nominal wind turbine mechanical output power (MW)	1.5
Power at point C (pu/mechanical power)	0.73
Wind speed at point C (m/s)	12
Pitch angle controller gain [Kp]	500
Maximum pitch angle (deg)	45
Maximum rate of change of pitch angle (deg/s)	2

TABLE III
EV DATA

Internal Resistor each Vehicle to plug in the Network (R_VSC)	0.02 (Ohm)
Internal admittance each Vehicle to plug in the Network (X_VSC)	1.4e-6 (Ohm)
Voltage for VSC to plug in the Network V_VSC	1.05 (pu)
Admittance for power transmission (Xs)	0.06 (pu)
Max SOC	0.99
Station parking capacity (kW)	2000
charging slot	5
DC voltage of charging slot (V)	200
maximum DC current of charging slot (A)	2

TABLE IV
MODULE DATA

Maximum Power (W)	414.8
Open circuit voltage Voc (V)	85.3
Temperature coefficient of Voc (%/deg.C)	-0.229
Short-circuit current Isc (A)	6.09
Temperature coefficient of Isc (%/deg.C)	0.030706

TABLE V
INVERTER DATA

Capacitance DC Link (F)	0.11
Internal Resistor each PV Module (R_PV)	0.038 (Ohm)
Internal admittance each PV Module (X_PV)	1.01e-6 (Ohm)
Voltage mag for PV Module V_PV	1.04 (pu)
Admittance for power transmission (Xs)	0.042 (pu)

TABLE VI
SPECIFICATION OF TEST CASES FOR PERFORMANCE EVALUATION OF THE PROPOSED SCHEME CONSIDERING HIGH PENETRATION OF WIND TURBINES

	Case 1	Case 2
Fault type	LLLG	LLLG
Fault location	10	26
Fault time initiation	0.1 s	0.1 s
Fault duration	0.1 s	0.15 s
Number of Wind Turbines (WT)	4	4
Number of Photovoltaic panels (PV)	2	2
Number of EV charging stations (EVS)	3	3

EV charging stations. The particle swarm optimization (PSO) algorithm is used to find the optimal solution [38].

The step time Δt for solving differential equations during the fault scenarios is selected 0.0001 s.

A. IEEE 69-Bus System Highly-Penetrated With Wind Farms

In order to validate the performance of the proposed scheme, two cases are provided in Table VI, where the following three conditions are investigated.

1) *Condition 1* (*C1*): No control action is applied on the EV charging stations.
2) *Condition 2* (*C2*): The proposed scheme is applied on the EV charging stations with the constraint on SoC that should not fall below 40% during each fault scenario.
3) *Condition 3* (*C3*): The proposed scheme is applied on the EV charging stations with no constraint on the SoC.

With the test cases introduced in Table VI, the numerical results of the rotor angle are presented in Figs. 6 and 7. As one can see in Fig. 6, the WT1, EVS1, and EVS3 become unstable in Case 1 and without considering the proposed scheme. However, applying the proposed scheme in C2 will result in only WT4 to become transiently unstable. As shown in Fig. 6(c), when there is no limitation enforced on the SoC discharge level, no generator instability is observed. For Case 2, according to Fig. 7, an instability of WT4 and EVS2 is observed, while utilizing the proposed scheme in C2 only results in the transient instability of WT4.

Additionally, focusing on C3, the proposed scheme with no constraints on the SoC discharge has resulted in the complete stability performance. From Figs. 6 and 7, it can be concluded that enforcing the constraints on the SoC level further restricts the optimization process and will lead to a lower control mechanism for managing the contributions of the EV charging stations during fault conditions.

In order to demonstrate the effectiveness of the proposed scheme in the entire active distribution network, it is essential to verify the ability of the proposed scheme in improving the transient stability margin of the entire grid.

In so doing, the probability density function (PDF) of critical clearing time (CCT) for the entire system can be employed [7]. PDF of CCT is recognized as a comprehensive index which can determine the overall stability margin of the whole network [7].

Utilizing random variables in [5] and [7], the PDF of CCT with/without considering the proposed scheme is calculated in 2000 Monte Carlo simulation scenarios. As it can be seen in Fig. 8, the PDF of CCTs considering C3 shows a significant rise in the system's transient stability margin.

B. IEEE 69-Bus System With High Penetration of PVs

Different from the previous case study, where WTs had a big portion of the system RES, this test case studies a scenario where the penetration of PVs is assumed greater than that of WTs. In other words, the mechanical inertia is reduced in comparison with the previous test case.

Similar to the previous test case, the performance of the proposed scheme is evaluated in two conditions provided in Table VII. For Case 1 in Table VII, the rotor angles in Fig. 9 demonstrate that WT1, PV2, EVS1, and EVS3 become unstable when the proposed control scheme is not applied. However, applying the proposed scheme in C2 has resulted in only PV2 to experiencing transient instability. Furthermore, according to Fig. 10, in Case 2 under C1, all RESs become unstable, while considering the proposed scheme under C2 results in only WT1, EVS1, and EVS3 becoming transiently unstable. The studied cases in this subsection highlighted that the high penetration of PVs results in less mechanical inertia. However, the proposed scheme is able to harness the role of converter connected RESs

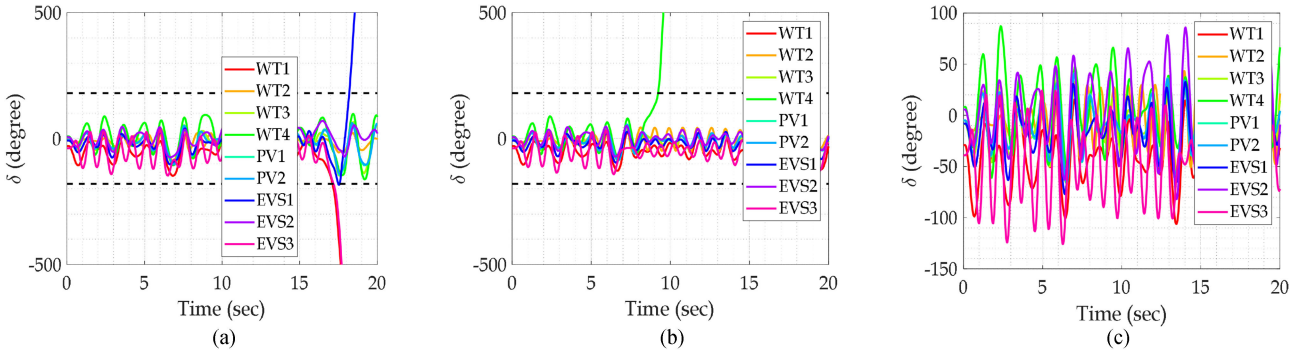

Fig. 6. Rotor angle for three cases given in Table I for a fault scenario at bus 10. (a) Without any control. (b) With the control scheme with SoC constraint. (c) With the control scheme with no SoC constraint.

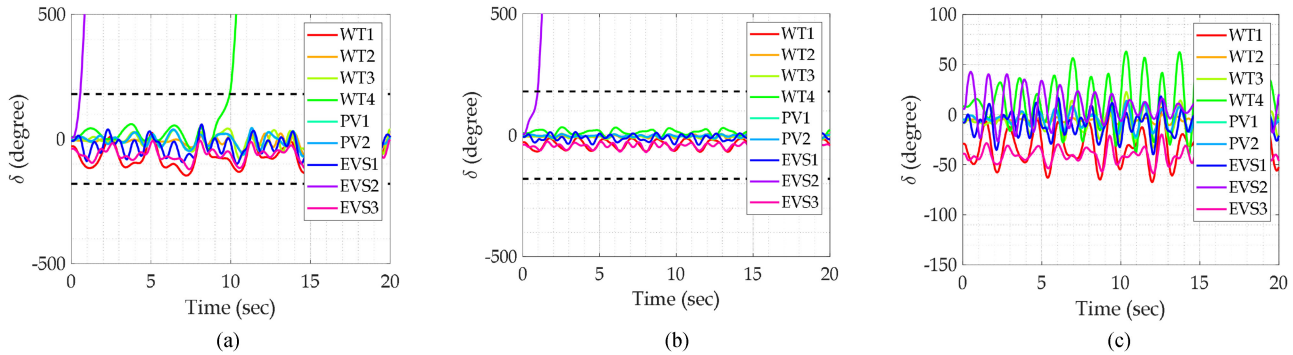

Fig. 7. Rotor angle for three cases given in Table I for a fault scenario at bus 26. (a) Without any control. (b) With the control scheme with SoC constraint. (c) With the control scheme with no SoC constraint.

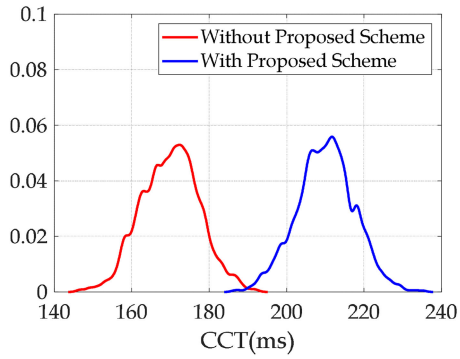

Fig. 8. PDF of CCT with/without considering the proposed scheme for the test system with four WTs, two PVs, and three EVS.

TABLE VII
SPECIFICATION OF TEST CASES FOR PERFORMANCE EVALUATION OF THE PROPOSED SCHEME WITH HIGH PENETRATION OF PVS

	Case 1	Case 2
Fault type	LLLG	LLLG
Fault location	5	18
Fault time initiation	0.1 s	0.1 s
Fault duration	0.2 s	0.25 s
Number of Wind Turbines (WT)	2	2
Number of Photovoltaic panels (PV)	4	4
Number of EV charging stations (EVS)	3	3

TABLE VIII
SPECIFICATION OF TEST CASES FOR PERFORMANCE EVALUATION OF THE PROPOSED SCHEME WITH HIGH PENETRATION OF PVS

	Case 1	Case 2
Fault type	LG	LG
Fault location	14	21
Fault time initiation	0.1 s	0.1 s
Fault duration	0.3 s	0.35 s
Number of Wind Turbines (WT)	1	1
Number of Photovoltaic panels (PV)	2	2
Number of EV charging stations (EVS)	1	1

in active distribution networks to preserve and even improve the transient stability performance across the network. As it can be seen in Fig. 11, the PDF of CCT for the test system with 2 WTs, 4 PVs, and 3 EVS shows an improvement in transient stability margin when the proposed scheme is applied.

C. IEEE 33-Bus System With High Penetration of PVs

Similar to the previous test case, the performance of the proposed scheme is evaluated under two conditions provided in Table VIII. The only difference is that the fault type is single line-to-ground (LG) fault. Note that the severity of LG fault is much less than LLLG fault type and it the most of case it may not lead to transient instability. However, for the cases provided

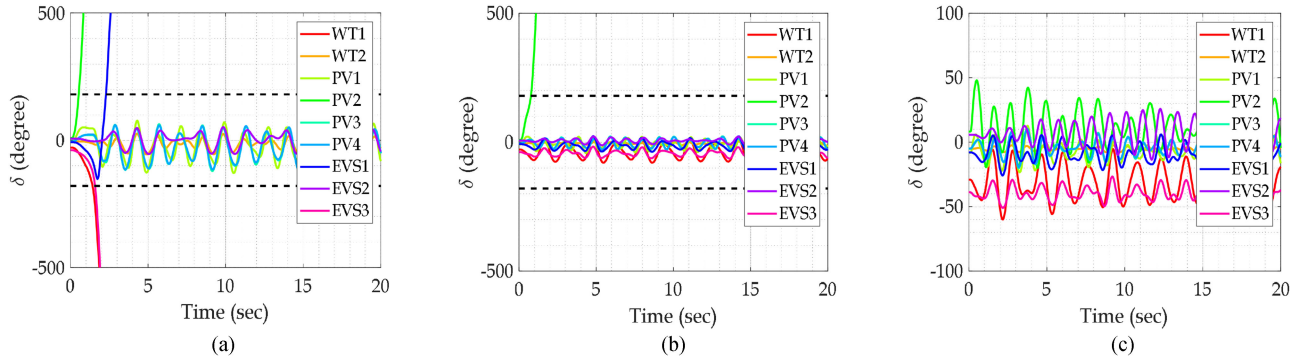

Fig. 9. Rotor angle for the three test cases given in Table II under a fault scenario at bus 5. (a) Without any control. (b) With the control scheme with SoC constraint. (c) With the control scheme with no SoC constraint.

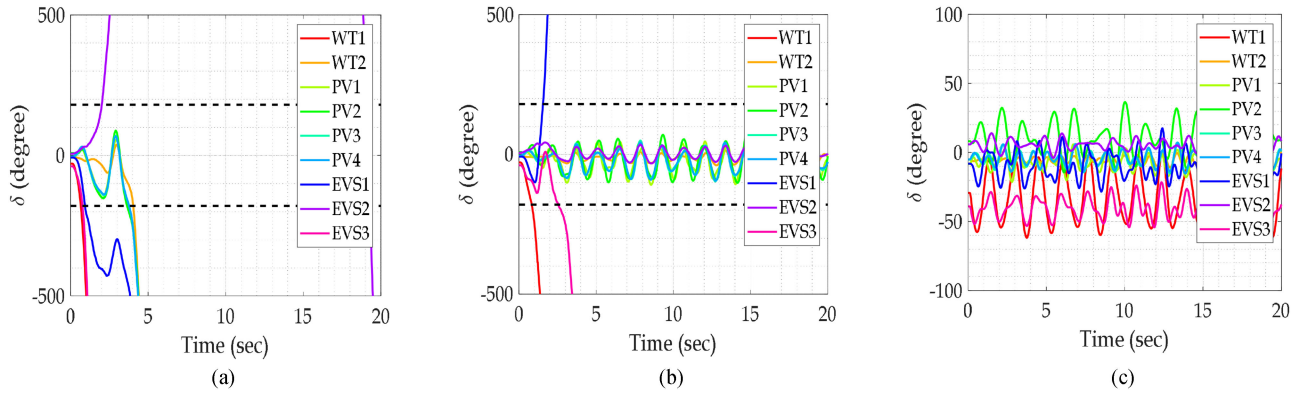

Fig. 10. Rotor angle for the three test cases given in Table II under a fault scenario at bus 18. (a) Without any control. (b) With the control scheme with SoC constraint. (c) With the control scheme with no SoC constraint.

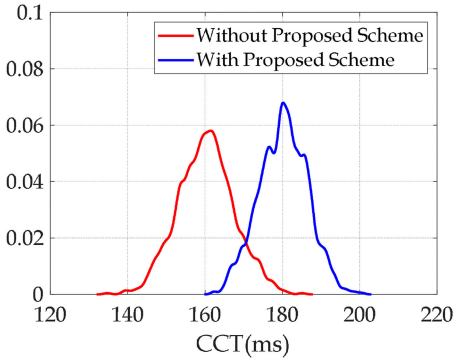

Fig. 11. PDF of CCT with/without considering the proposed scheme for the test system with two WTs, four PVs, and three EVS.

in the Table VIII, transient instability has happened. For Case 1 in Table VII, the rotor angles in Fig. 12 demonstrate that all units become unstable when the proposed control scheme is not applied. Even applying the proposed scheme in C2 has not resulted transient stability of any units. However, applying proposed scheme in C3 makes the system fully stable. Same result is concluded for Case 2 from Fig. 13 considering applying proposed scheme in C3.

The results of this case indicate that regardless of fault type condition, the proposed scheme can control the contribution EVS so that the kinetic energy of the whole system does not reach to critical value and consequently the system remains transiently stable.

D. IEEE 119-Bus Test System

In this section, the proposed approach is applied on the IEEE 119-bus test system with the following two scenarios.

1) *Scenario 1:* system contains seven WTs, three PVs, and five EVS.
2) *Scenario 2:* system contains three WTs, seven PVs, and five EVS.

For both scenarios, PDFs of CCT are assessed and demonstrated in Figs. 14and 15. As it can be seen in both figures, the transient stability margin of the network is generally improved. However, in the scenario with high penetration of PVs, the mechanical inertia and the CCT demonstrating the transient stability margin are significantly less than those in the scenario with lower penetration of PVs.

To show the impact of SoC constraint on the performance of the proposed algorithm, some different constraints are considered which is tabulated in Table IX. Note that the number of DGs is in accordance with scenario 2.

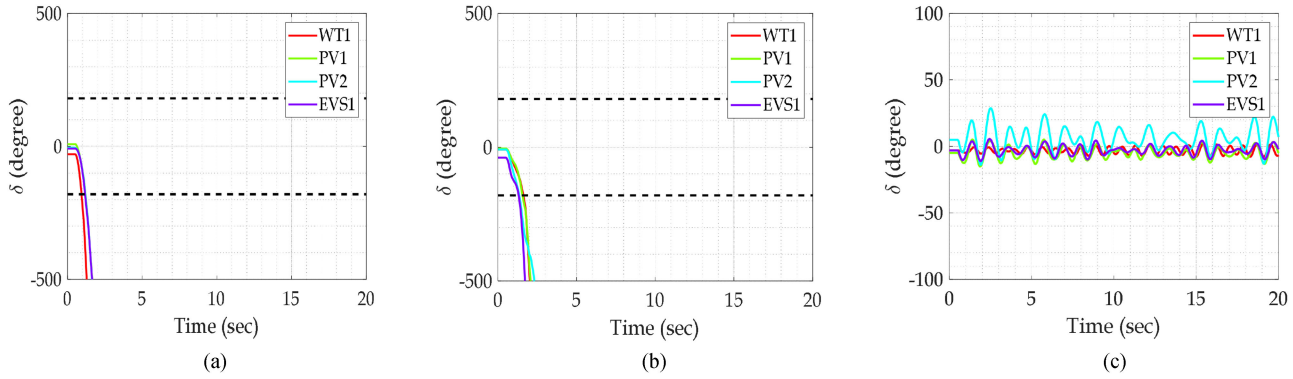

Fig. 12. Rotor angle for the three test cases given in Table III under a fault scenario at bus 14. (a) Without any control. (b) With the control scheme with SoC constraint. (c) With the control scheme with no SoC constraint.

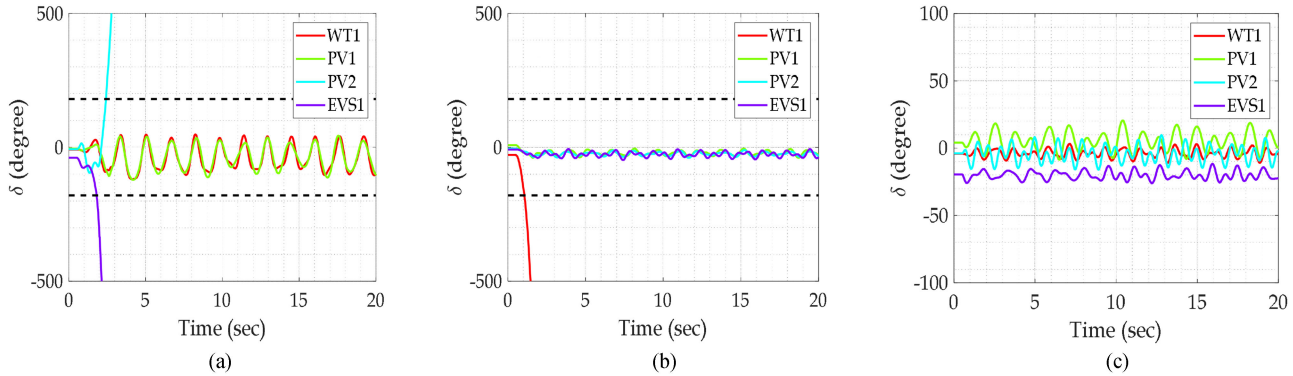

Fig. 13. Rotor angle for the three test cases given in Table III under a fault scenario at bus 21. (a) Without any control. (b) With the control scheme with SoC constraint. (c) With the control scheme with no SoC constraint.

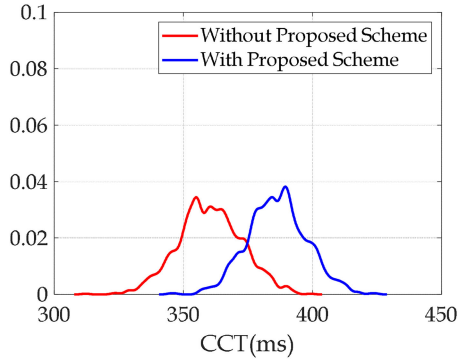

Fig. 14. PDF of CCT with/without considering the proposed scheme for the test system with seven WTs, three PVs, and five EVS.

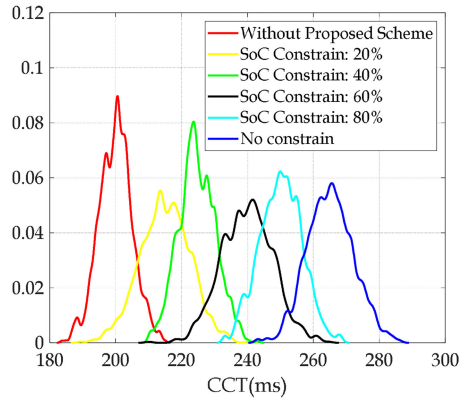

Fig. 15. PDF of CCT with/without considering the proposed scheme for the test system with three WTs, seven PVs, and five EVS.

TABLE IX
SPECIFICATION OF CONSTRAINS FOR PERFORMANCE EVALUATION OF THE PROPOSED SCHEME FOR SCENARIO 2

SoC Constrain	Upper Limit	Lower Limit
Without Proposed Scheme	-	-
20%	100%	80%
40%	100%	60&
60%	100%	40%
80%	100%	20%
No Constrain	100%	0%

According to Fig. 16, as the limitation on the SoC decreases, the proposed method is able to control the contributions of EVs during fault scenarios and as a result, the CCT of the system becomes larger. Therefore, by increasing the SoC constrain, the PDF of CCT moves to the right side which means the transient stability margin of the whole system is improved.

Increasing the number of PVs and EVSs comparing with WT will deteriorate the transient stability of the system. This issue is

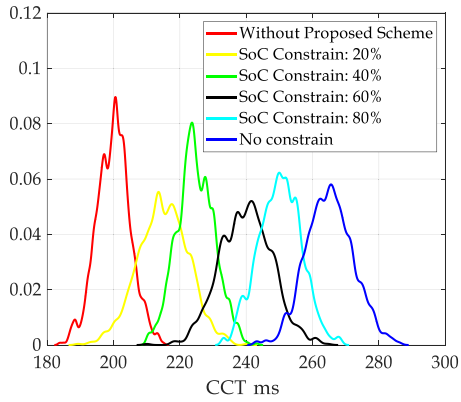

Fig. 16. PDF of CCT for evaluating the performance of the proposed scheme considering different constraints for the test system with three WTs, seven PVs, and five EVS.

TABLE X
COMBINATIONS OF PVS, EVSS, AND WTS FOR PERFORMANCE EVALUATION OF THE PROPOSED SCHEME

Combination (Comb)	Number of Wind Turbines (WT)	Number of Photovoltaic panels (PV)	Number of EV charging stations (EVS)
1	2	8	5
2	3	8	4
3	4	6	5
4	5	6	4
5	6	4	5
6	7	4	4
7	8	2	5

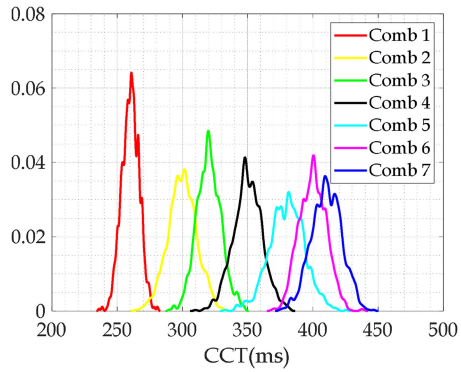

Fig. 17. PDF of CCT for evaluating the performance of the proposed scheme considering different combinations of PVs, EVSs, and WTs.

shown in the Figs. 14 and 15. To more effectively investigating the impact of number of PVs and EVSs on the transient stability deterioration, some combinations of PVs, EVSs and WTs, are provided in Table X. It should be noted that during this investigation no constrain is considered for SoC. According to Table X and Fig. 17, it is observed that by increasing the number of PVs and EVSs, the PDFs of CCT move toward the left which means the stability of the system notably deteriorates.

TABLE XI
REQUIREMENTS OF OPTIMIZATION ALGORITHMS

Algorithm	Population size	Dimensions	Maximum iteration	Stopping Time Limit (Se)
PSO	12	45	150	inf
DE	12	45	150	inf
BBO	12	45	150	inf

TABLE XII
RESULTS OF DIFFERENT OPTIMIZATION ALGORITHMS FOR SCENARIOS TABLE VI

	Case 1		Case 2	
	C1	C3	C1	C3
PSO	WT1, EVS1,EVS3	No Instability	WT4, EVS2	No Instability
DE	WT1, EVS1,EVS3	PV1	WT4, EVS2	No Instability
BBO	WT1, EVS1,EVS3	No Instability	WT4, EVS2	No Instability

TABLE XIII
RESULTS OF DIFFERENT OPTIMIZATION ALGORITHMS FOR SCENARIOS TABLE VII

	Case 1		Case 2	
	C1	C3	C1	C3
PSO	WT1, PV2, EVS1,EVS3	No Instability	All Units unstable	No Instability
DE	WT1, PV2, EVS1,EVS3	PV2	All Units unstable	WT3
BBO	WT1, PV2, EVS1,EVS3	No Instability	All Units unstable	No Instability

TABLE XIV
RESULTS OF DIFFERENT OPTIMIZATION ALGORITHMS FOR SCENARIOS TABLE VIII

	Case 1		Case 2	
	C1	C3	C1	C3
PSO	PV2, EVS1	No Instability	All Units unstable	No Instability
DE	PV2, EVS1	PV2	All Units unstable	No Instability
BBO	PV2, EVS1	No Instability	All Units unstable	No Instability

E. Performance of the Proposed Scheme With Different Optimization Algorithms

This section is dedicated to evaluation of the performance of the proposed scheme with different optimization algorithms. To such aim, three optimization algorithms are utilized to solve the proposed optimization algorithm. The utilized optimization algorithms contain PSO [38], differential evolutionary (DE) [39], and biogeography-based optimization (BBO) [40]. The implementation requirements of these algorithms are provided in Table XI. Six cases given in Tables VI to VIII are fed to optimization algorithms and the numerical results are provided in Tables XII to XIV.

According to the results of the different optimization algorithms, it is observed that PSO and BBO are successfully solved the problem since the results of these algorithms are in accordance with time domain simulation. However, DE algorithm has failed in some cases comparing to the time domain simulation results.

The simulation results and discussions demonstrated that the proposed scheme is able to effectively deal with the challenge of transient stability deterioration with the contributions made from the converter connected RESs. The proposed control strategy finds an optimized solution in which the contribution of EV charging stations plays a positive role in reducing the rate of change of the kinetic energy and simultaneously increasing the margin for the total CKE. In fact, the proposed strategy controls the RESs converters and depresses the negative impacts of a lower mechanical inertia in the active distribution network with high penetration of converter-interfaced RESs.

The proposed method can be used as auxiliary program in simulation software in planning stage to evaluate the preserving ability of the system in different contingencies and providing different back-up strategies that can be helpful to maintain stability of the system. Also with proper communication infrastructures for data transmission, the proposed algorithm can be employed in local smart grid control center to perform real-time control on the contribution of EVs and other fast ESSs so that the power grids can maintain transient stability.

V. Conclusion

With the rushing arrival of the converter-interfaced RESs replacing the conventional rotational generators, the dynamic security of the active distribution grids is heavily impacted. This article provided an objective function to deal with the negative effects of EV charging stations on the transient stability margin in active distribution networks. The objective function was designed to control the SoC of EV charging stations based on the concept of VSG to assess the TCCKE of the network during fault scenarios. Analyzing the proposed scheme on the standard IEEE distribution test systems under different fault conditions, it was observed that the proposed scheme could improve the transient stability margin. The simulation results demonstrated that the proposed scheme (with/without SoC constraints) could improve the system stability compared to the conditions where EV charging stations were not controlled during fault scenarios. Also, high penetration of PV and the resulting reduction in the system mechanical inertia would lead to loss of synchronism very quickly. However, the proposed control scheme could control the DERs' contributions in order to minimize the transient instability. The PDFs of CCT illustrated the effectiveness of the proposed scheme in an overall improvement of the transient stability margin considering different penetration levels of wind and PV resources. The proposed scheme could minimize the deterioration effects of converter-interfaced RESs on the transient stability of active distribution networks.

Future work can be dedicated to combine the proposed algorithm with optimal allocation of RESs and ESSs to find the allowable number of converter- interfaced RESs and ESSs in the network while transient stability is preserved.

References

[1] S. Senemar, M. Rastegar, M. Dabbaghjamanesh, and N. D. Hatziargyriou, "Dynamic structural sizing of residential energy hubs," *IEEE Trans. Sustain. Energy*, vol. 11, no. 3, pp. 1236–1246, Jul. 2020.

[2] S. Senemar, A. R. Seifi, M. Rastegar, and M. Parvania, "Probabilistic optimal dynamic planning of onsite solar generation for residential energy hubs," *IEEE Syst. J.*, vol. 14, no. 1, pp. 832–841, Mar. 2020.

[3] G. Magdy, E. A. Mohamed, G. Shabib, A. A. Elbaset, and Y. Mitani, "Microgrid dynamic security considering high penetration of renewable energy," *Protection Control Modern Power Syst.*, vol. 3, no. 1, 2018, Art. no. 23.

[4] E. Rokrok, M. Shafie-Khah, and J. P. Catalão, "Review of primary voltage and frequency control methods for inverter-based islanded microgrids with distributed generation," *Renewable Sustain. Energy Rev.*, vol. 82, pp. 3225–3235, 2018.

[5] M. Tajdinian, M. Allahbakhshi, M. Mohammadpourfard, B. Mohammadi, Y. Weng, and Z. Dong, "Probabilistic framework for transient stability contingency ranking of power grids with active distribution networks: Application in post disturbance security assessment," *IET Gener., Transmiss. Distrib.*, vol. 14, no. 5, pp. 719–727, Mar. 2020.

[6] M. Z. Jahromi, M. Tajdinian, J. Zhao, P. Dehghanian, M. Allahbakhsi, and A. R. Seifi, "Enhanced sensitivity-based decentralised framework for real-time transient stability assessment in bulk power grids with renewable energy resources," *IET Gener., Transmiss. Distrib.*, vol. 14, no. 4, pp. 665–674, Feb. 2020.

[7] M. Tajdinian, A. R. Seifi, and M. Allahbakhshi, "Calculating probability density function of critical clearing time: Novel formulation, implementation and application in probabilistic transient stability assessment," *Int. J. Elect. Power Energy Syst.*, vol. 103, pp. 622–633, 2018.

[8] M. Tajdinian, A. R. Seifi, and M. Allahbakhshi, "Transient stability of power grids comprising wind turbines: New formulation, implementation, and application in real-time assessment," *IEEE Syst. J.*, vol. 13, no. 1, pp. 894–905, Mar. 2018.

[9] M. Tajdinian, A. R. Seifi, and M. Allahbakhshi, "Sensitivity-based approach for real-time evaluation of transient stability of wind turbines interconnected to power grids," *IET Renewable Power Gener.*, vol. 12, no. 6, pp. 668–679, Apr. 2018.

[10] B. Zhou, T. Littler, and L. Meegahapola, "Assessment of transient stability support for electric vehicle integration," in *Proc. IEEE Power Energy Soc. General Meeting*, 2016, pp. 1–5.

[11] A. Gajduk, M. Todorovski, J. Kurths, and L. Kocarev, "Improving power grid transient stability by plug-in electric vehicles," *New J. Phys.*, vol. 16, no. 11, 2014, Art. no. 115011.

[12] V. R. Pandi, A. Al-Hinai, and A. Feliachi, "Coordinated control of distributed energy resources to support load frequency control," *Energy Convers. Manage.*, vol. 105, pp. 918–928, 2015.

[13] N. Rezaei and M. Kalantar, "Stochastic frequency-security constrained energy and reserve management of an inverter interfaced islanded microgrid considering demand response programs," *Int. J. Elect. Power Energy Syst.*, vol. 69, pp. 273–286, 2015.

[14] M. Chen and X. Xiao, "Hierarchical frequency control strategy of hybrid droop/VSG-based islanded microgrids," *Elect. Power Syst. Res.*, vol. 155, pp. 131–143, 2018.

[15] N. Rezaei and M. Kalantar, "Hierarchical energy and frequency security pricing in a smart microgrid: An equilibrium-inspired epsilon constraint based multi-objective decision making approach," *Energy Convers. Manage.*, vol. 98, pp. 533–543, 2015.

[16] S. M. B. Sadati, J. Moshtagh, M. Shafie-khah, A. Rastgou, and J. P. Catalão, "Bi-level model for operational scheduling of a distribution company that supplies electric vehicle parking lots," *Elect. Power Syst. Res.*, vol. 174, 2019, Art. no. 105875.

[17] S. M. B. Sadati, J. Moshtagh, M. Shafie-khah, A. Rastgou, and J. P. Catalão, "Operational scheduling of a smart distribution system considering electric vehicles parking lot: A bi-level approach," *Int. J. Elect. Power Energy Syst.*, vol. 105, pp. 159–178, 2019.

[18] Y. Geng and C. G. Cassandras, "New "smart parking," system based on resource allocation and reservations," *IEEE Trans. Intell. Transp. Syst.*, vol. 14, no. 3, pp. 1129–1139, Sep. 2013.

[19] Q. Chen, N. Liu, C. Hu, L. Wang, and J. Zhang, "Autonomous energy management strategy for solid-state transformer to integrate PV-assisted EV charging station participating in ancillary service," *IEEE Trans. Ind. Inform.*, vol. 13, no. 1, pp. 258–269, Feb. 2017.

[20] Y. Yang, S. Bremner, C. Menictas, and M. Kay, "Battery energy storage system size determination in renewable energy systems: A review," *Renewable Sustain. Energy Rev.*, vol. 91, pp. 109–125, 2018.

[21] X. Zhu, M. Xia, and H.-D. Chiang, "Coordinated sectional droop charging control for EV aggregator enhancing frequency stability of microgrid with high penetration of renewable energy sources," *Appl. Energy*, vol. 210, pp. 936–943, 2018.

[22] K. S. El-Bidairi, H. D. Nguyen, T. S. Mahmoud, S. Jayasinghe, and J. M. Guerrero, "Optimal sizing of battery energy storage systems for dynamic frequency control in an islanded microgrid: A case study of Flinders island, Australia," *Energy*, vol. 195, 2020, Art. no. 117059.
[23] M. H. Ali, B. Wu, and R. A. Dougal, "An overview of SMES applications in power and energy systems," *IEEE Trans. Sustain. Energy*, vol. 1, no. 1, pp. 38–47, Apr. 2010.
[24] M. H. Ali, T. Murata, and J. Tamura, "A fuzzy logic-controlled superconducting magnetic energy storage for transient stability augmentation," *IEEE Trans. Control Syst. Technol.*, vol. 15, no. 1, pp. 144–150, Jan. 2007.
[25] M. Hojo, Y. Mitani, and K. Tsuji, "Linearization of generator power swing property by controlling power output of SMES for enhancement of power system stability," *IEEE Trans. Appl. Supercond.*, vol. 9, no. 2, pp. 338–341, Jun. 1999.
[26] S. Nomura, T. Shintomi, S. Akita, T. Nitta, R. Shimada, and S. Meguro, "Technical and cost evaluation on SMES for electric power compensation," *IEEE Trans. Appl. Supercond.*, vol. 20, no. 3, pp. 1373–1378, Jun. 2010.
[27] D. Wu, K. T. Chau, C. Liu, S. Gao, and F. Li, "Transient stability analysis of SMES for smart grid with vehicle-to-grid operation," *IEEE Trans. Appl. Supercond.*, vol. 22, no. 3, Jun. 2012, Art. no. 5701105.
[28] A. Ghosh, R. Patel, M. Datta, and L. Meegahapola, "Investigation of transient stability of a power network with solar-PV generation: Impact of loading level & control strategy," in *Proc. IEEE Innov. Smart Grid Technol.*, 2017, pp. 1–6.
[29] S. Eftekharnejad, V. Vittal, G. T. Heydt, B. Keel, and J. Loehr, "Impact of increased penetration of photovoltaic generation on power systems," *IEEE Trans. Power Syst.*, vol. 28, no. 2, pp. 893–901, May 2013.
[30] A. Ortega and F. Milano, "Generalized model of VSC-based energy storage systems for transient stability analysis," *IEEE Trans. Power Syst.*, vol. 31, no. 5, pp. 3369–3380, Sep. 2016.
[31] S. Wang, Z. Liu, and J. Liu, "Modeling of D-Q small-signal impedance of virtual synchronous generator," in *Proc. IEEE Int. Power Electron. Application Conf. Expo.*, 2018, pp. 1–6.
[32] S. D'Arco, J. A. Suul, and O. B. Fosso. "Small-signal modeling and parametric sensitivity of a virtual synchronous machine in islanded operation," *Int. J. Elect. Power Energy Syst.*, vol. 72, pp. 3–15, 2015.
[33] B. Gao, C. Xia, N. Chen, K. M. Cheema, L. Yang, and C. Li, "Virtual synchronous generator based auxiliary damping control design for the power system with renewable generation," *Energies*, vol. 10, no. 8, 2017, Art. no. 1146.
[34] V. MATLAB, *9.4. 0 (R2018a)*. Natick, MA, USA: MathWorks Inc.: 2018.
[35] W. A. Vasquez and F. L. Quilumba, "Load flow method for radial distribution systems with distributed generation using a dynamic data matrix," in *Proc. IEEE Ecuador Tech. Chapters Meeting*, 2016, pp. 1–5.
[36] M. Nayeripour, E. Mahboubi-Moghaddam, J. Aghaei, and A. Azizi-Vahed, "Multi-objective placement and sizing of DGs in distribution networks ensuring transient stability using hybrid evolutionary algorithm," *Renewable Sustain. Energy Rev.*, vol. 25, pp. 759–767, 2013.
[37] A. Ehsan and Q. Yang, "Optimal integration and planning of renewable distributed generation in the power distribution networks: A review of analytical techniques," *Appl. Energy*, vol. 210, pp. 44–59, 2018.
[38] M. H. Hemmatpour and M. Mohammadian, "An evolutionary approach for optimum reconfiguration and distributed generation planning considering variable load pattern based on voltage security margin," *Arabian J. Sci. Eng.*, vol. 38, no. 12, pp. 3407–3420, 2013.
[39] K Y. Lee and M. A. El-Sharkawi, Eds. *Modern Heuristic Optimization Techniques: Theory and Applications to Power Systems*, vol. 39. Hoboken, NJ, USA: Wiley, 2008.
[40] C. A. Coello and G. B. Lamont, *Applications of Multi-Objective Evolutionary Algorithms*, vol. 1. World Scientific: Singapore, 2004.